mathematics

MDPI

Article

Semi-Analytical Pricing of Barrier Options in a Hybrid Model of Stochastic and Local Volatility

Jiling Cao, Sheng Gong, Xi Li and Wenjun Zhang *

Department of Mathematical Sciences, School of Engineering, Computer and Mathematical Sciences, Auckland University of Technology, Private Bag 92006, Auckland 1142, New Zealand; jiling.cao@aut.ac.nz (J.C.); sheng.gong@aut.ac.nz (S.G.); xi.li@aut.ac.nz (X.L.)
* Correspondence: wenjun.zhang@aut.ac.nz

Abstract

In this paper, the valuation of barrier options is studied when the underlying asset is driven by a hybrid model of stochastic volatility and constant elasticity of variance. Using an asymptotic expansion approach and the Fourier transform method, a semi-analytical approximate pricing formula for up-and-out call options are derived under the proposed hybrid model. We validate the approximate pricing formula by comparing its outputs with those produced by Monte Carlo simulation and the binomial tree method. In addition, we perform a sensitivity analysis numerically on the key model parameters and investigate limiting regimes of the hybrid model. It is verified that the approximation is properly anchored to simpler benchmark models when one or both perturbative effects vanish.

Keywords: asymptotic; barrier option; elasticity of variance; stochastic volatility; up-and-out call; Fourier transform

MSC: 91G20; 91G15; 35B25; 60J76; 42B10

1. Introduction

Financial derivatives play an essential role in hedging against risk and the valuation of derivatives in an appropriate model specification when the dynamics of the underlying asset is of fundamental importance. Barrier options are regarded as one of the most popular types of path-dependent options among various financial derivatives. Unlike standard vanilla options whose payoffs depend solely on the terminal value of the underlying equity at maturity, the payoff structures of barrier options depend on the entire path evolution of the underlying equity over the contract period. Therefore, the pricing of barrier options is considerably more complex than that of European options. In the literature, this topic has been investigated in various models, among which the earliest example is the work of Merton in [1]. In Merton's research, a closed-form pricing formula for the down-and-out barrier call option is derived under the framework of geometric Brownian motion (i.e., the Black–Scholes model framework), which is an extension of the classical European option pricing formula under the Black–Scholes model [2]. Later, Reiner and Rubinstein [3] developed explicit formulae for the prices of all other types of barrier options.

It is widely known that the assumption of constant volatility in the classical framework of the geometric Brownian motion model is controversial to the existing empirical evidence which shows that the time series of volatility is highly variable and difficult to predict over time. Therefore, it is more reasonable to treat the volatility as a variable or stochastic factor.

Academic Editor: Anatoliy Swishchuk

Received: 27 April 2026
Revised: 12 May 2026
Accepted: 12 May 2026
Published: 13 May 2026

In this regard, "local volatility" and "stochastic volatility" are considered as two widely used continuous-time approaches to extend the classical geometric Brownian motion model. In the literature, the constant elasticity of variance (CEV) model introduced in [4] is considered as one of the most commonly adopted local volatility models, and the stochastic volatility (SV) model developed by Heston in [5], known as the Heston model, is considered as a foundational and "legendary" model in quantitative finance. Both models provide a closed-form analytic solution to the pricing of European options.

In 1999, Boyle and Tian [6] evaluated barrier options in the CEV model by approximating the CEV process using a trinomial process. Davydov and Linetsky [7] later derived explicit formulae for the price of barrier options under the CEV model. In real financial markets, most barrier options are monitored discretely on the basic of daily, weekly, or monthly dates. Motivated by this observation, Thakoor et al. [8] investigated the pricing of continuously and discretely monitored barriers in the CEV model. They discovered that continuously monitored barriers admit an analytical solution, while the evaluation process through this formula remains non-trivial. This means that discretely observed barriers must be priced numerically. Their major contribution is to propose a fourth-order numerical scheme for the pricing of continuously and discretely monitored barriers in the CEV model. Further along this direction, Carr et al. [9] considered the pricing of Barrier options in the time-dependent CEV and CIR models. Using two different but complementary approaches ("the method of Bessel potentials" and "the method of generalized integral transform"), they solved the problem of pricing a down-and-out put option in the time-dependent CIR and CEV models in semi-closed form, and then the option price is represented as a one-dimensional integral.

In general, analytical expressions of barrier options under stochastic volatility models are unavailable under stochastic volatility models. A numerical algorithm was applied by Chiarella et al. [10] to approximate the value of barrier options when the dynamics of the underlying assets follows the Heston model. A semi-closed form expression for up-and-out barrier options was derived by Kato et al. [11] under a class of stochastic volatility models, including the SABR model [12]. A general integral transform (GIT) method for pricing the down-and-out put barrier options under a time-dependent Heston model with a time-dependent barrier was developed by Carr et al. [13], and a semi-analytical solution that is expressed in a two-dimensional integral was also derived for this problem. Further, He and Lin [14] considered the pricing of continuously monitored barrier options in the Heston stochastic volatility model. They developed a two-step solution process and presented an analytical approximation formula that is of high efficiency and accuracy. This two-step solution process splits the complex task of pricing barrier options under the Heston model into two small parts which are relatively easier to solve.

In 2023, Cao et al. [15] considered the valuation of barrier options under a hybrid framework combining the SV and CEV features. They derived a semi-closed form formula for down-and-out put barrier options in their model framework using the Mellin transform approach. In this paper, we continue to work along this line, but we focus on other types of barrier options. The main contribution of this article is to give a new semi-closed form approximation pricing formula for up-and-out call options in a hybrid model of the CEV model and a general type of stochastic volatility model introduced in [16] using the Fourier transform method. In addition, numerical experiments regarding validation and sensitivity analysis of the semi-closed form solution are implemented.

The rest of this paper is organized as follows. In Section 2, we introduce the model framework and give a general description of eight main types of single-barrier options, which are classified based on whether they are activated ("in") or deactivated ("out") when the underlying asset price hits a specific barrier level. Then, we focus on the up-and-out call (UOC)

options and derive a governing PDE for the premium of this type of barrier options under our model framework. In Section 3, we discuss an asymptotic method for obtaining pricing approximations of UOC options and give a semi-closed form approximate pricing formula consisting of the zero-order and first-order correction terms. In Section 4, we implement numerical experiments. First, we compare the numerical results from the semi-closed form pricing formulae with those generated by Monte Carlo simulations, which demonstrates the accuracy of the pricing formula. We also compute the up-and-out barrier-option prices by the binomial tree method proposed in [17] and compare the computational efficiency and relative errors among our semi-close pricing formula, Monte Carlo simulation, and the binomial tree method. Second, to test the robustness of our approach, we conduct sensitivity analysis on the UOC option price with respect to three perturbation parameters, namely, ϵ, β, and m. Third, we investigate three limiting regimes of the model when one or both perturbative effects vanish. This allows us to validate whether the approximation is properly anchored to simpler benchmark models. Finally, we provide some discussions which highlight our numerical findings. In Section 5, we give a summary of this paper.

2. Model Framework and Barrier Options

2.1. A Hybrid Stochastic and Local Volatility Model

Let $\{S_t : t \geq 0\}$ be the price process of a risky equity on a filtered probability space $(\Omega, \mathscr{F}, (\mathscr{F}_t)_{t\geq 0}, \mathbb{Q})$, where $\mathbb{Q}$ is a risk-neutral probability measure. We assume that $\{S_t : t \geq 0\}$ follows the dynamics described by the following system:

$$\begin{aligned} dS_t &= rS_t\,dt + f(Y_t)S_t^{1+\beta}\,dW_t^s, \\ dY_t &= \alpha(m - Y_t)\,dt + \gamma dW_t^y, \end{aligned} \tag{1}$$

where $\alpha > 0$, $\gamma > 0$, m, and β are constants, $r > 0$ is the risk-free interest rate, and f is a function of the unobserved process $\{Y_t : t \geq 0\}$ to determine the volatility. The processes $\{W_t^s : t \geq 0\}$ and $\{W_t^y : t \geq 0\}$ are correlated standard Brownian motions under $\mathbb{Q}$, with the correlation coefficient $\rho \in (-1, 1)$. The parameter β represents the elasticity of variance and is typically small in empirical studies such as [18]. It is empirically observed that $\beta < 0$ in equity markets.

Note that $\{Y_t : t \geq 0\}$ is a mean-reverting process with long-term mean m, mean reversion speed α, and volatility γ. The system in (1) represents a hybrid model of stochastic volatility (SV) and constant elasticity of variance (CEV) (local volatility). Hence, it is referred to as the *SVCEV model*, which was firstly applied in [16] to the valuation of European options and was later applied to the valuation of variance swaps in [19]. In (1), f is assumed to be bounded and sufficiently smooth. We do not need to specify a functional form of f until Section 4, where f takes a specific form as that used in [15,20,21].

The process $\{Y_t : t \geq 0\}$ is an Ornstein—Uhlenbeck (OU) process with an invariant distribution, which is normal with mean m and variance $\gamma^2/(2\alpha)$. Thus, when $\beta \to 0$ and $\alpha \to \infty$, the equity process approaches to geometric Brownian motion and thus the Black–Scholes model becomes a good approximation of the SVCEV model. However, for merely fast (not infinite) mean reversion and small (not negligible) elasticity of variance, stochastic volatility effects remain important. To capture these corrections, we follow [20] to introduce the small parameter $\varepsilon = 1/\alpha$ and define $\nu = \gamma/\sqrt{2\alpha}$. With these notations, the dynamics under $\mathbb{Q}$ can be re-written as

$$\begin{aligned} dS_t &= rS_t\,dt + f(Y_t)S_t^{1+\beta}\,dW_t^s, \\ dY_t &= \frac{1}{\varepsilon}(m - Y_t)dt + \frac{\sqrt{2}\nu}{\sqrt{\varepsilon}}\,dW_t^y. \end{aligned} \tag{2}$$

We apply the log transform of the equity price by setting $X_t := \ln S_t$. Then, by applying Itô's lemma, we can derive the dynamics of log equity price X_t from (1) as follows:

$$\begin{aligned} dX_t &= \left(r - \frac{1}{2}f^2(Y_t)\right)dt + f(Y_t)e^{\beta X_t}\,dW_t^x, \\ dY_t &= \frac{1}{\varepsilon}(m - Y_t)dt + \frac{\sqrt{2}\nu}{\sqrt{\varepsilon}}\,dW_t^y. \end{aligned} \tag{3}$$

In the sequel, we will study the valuation problem of barrier options under the SVCEV model (1). Through the transformed price dynamics in (2) and (3), by employing an asymptotic approach and Fourier transform method, we are able to derive a semi-analytical approximation pricing formula for up-and-out call options.

2.2. Barrier Options

In this subsection, we recall the basic features of eight main types of (single) barrier options, namely up-and-out calls and puts, down-and-out calls and puts, up-and-in calls and puts, and down-and-in calls and puts. An *up-and-out call* (UOC) option gives the holder the right to buy an asset at a strike price, but becomes worthless ("knocks out") if the asset's price rises to or exceeds a specific, predetermined barrier level during the option's life. Similarly, a *down-and-out call* (DOC) option is a barrier option that becomes worthless if the asset's price falls to a predetermined level. In contrast, an *up-and-in call* (UIC) option only becomes active (or "knock in") if the underlying asset's price rises to a specified barrier level during the option's life. If the price never hits the barrier, the option expires worthless. Similarly, a *down-and-in call* (DIC) only comes into existence ("knock in") if the underlying asset's price falls to a specific, predetermined barrier level during the option's life. Otherwise, it expires worthless. Concepts of the corresponding put options can be defined accordingly.

Note that in the absence of any rebates, the relationship between an 'in' barrier option and an 'out' barrier option (with the same payoff and same barrier level) is simply given by

$$\text{in} + \text{out} = \text{vanilla}. \tag{4}$$

Due to this relationship, we are able to value an 'in' (or 'out') barrier option under a model once we know how to value an 'out' (or 'in') barrier option (with the same payoff and same barrier level) under the the same model. In [15], Cao et al. derived a semi-closed form of pricing formula for down-and-out put options in the SVCEV model. Applying the put–call parity, the relationship in (4), and the pricing formula of vanilla call options in [16], we are able to work out the valuation of down-and-out call, down-and-in call, and down-and-in put options. This leaves the valuation of the remaining four types of barrier options untouched under the SVCEV model. Hence, in the sequel, we focus only on the valuation of up-and-out call options on a risky equity, whose price dynamics follow Equation (2).

For notational convenience, at any time $0 \le t \le T$, where T denotes the expiry time of an up-and-out call option on $\{S_t : t \ge 0\}$, we define the running minimum U_t and maximum Z_t of the log-price process $\{X_t : 0 \le t \le T\}$ by

$$U_t := \min\{X_u : 0 \le u \le t\} \qquad \text{and} \qquad Z_t := \max\{X_u : 0 \le u \le t\}.$$

The payoff of an up-and-out call option with log-strike k and log-barrier level b (with $0 < k < b$) is given by

$$\mathrm{UOC}(X_T) = \max\Big\{e^{X_T} - e^k,\, 0\Big\}\, \mathbb{1}_{\{Z_T < b\}},$$

where $\mathbb{1}_{\{Z_T<b\}}$ is the indicator function which shows that the log-price has never crossed the barrier before maturity. Under the SVCEV model framework, the risk-neutral price of an up-and-out call option at time $t \in [0, T]$ is

$$P^{\beta,\varepsilon}(t,x,y) = e^{-r(T-t)}\mathbb{E}^{\mathbb{Q}}\big[\mathrm{UOC}(X_T) \,\big|\, X_t = x,\ Y_t = y\big].$$

Applying the Feynman–Kac theorem, we can obtain the following two-dimensional partial differential equation (PDE):

$$\begin{aligned} 0 = {} & \frac{\partial P^{\beta,\varepsilon}}{\partial t} + \frac{1}{2}e^{2\beta x} f^2(y)\frac{\partial^2 P^{\beta,\varepsilon}}{\partial x^2} + \Big(r - \tfrac{1}{2}f^2(y)\Big)\frac{\partial P^{\beta,\varepsilon}}{\partial x} \\ & + \frac{\sqrt{2}\,\rho\,\nu\, e^{\beta x}}{\sqrt{\varepsilon}} f(y)\,\frac{\partial^2 P^{\beta,\varepsilon}}{\partial x\,\partial y} + \frac{\nu^2}{\varepsilon}\frac{\partial^2 P^{\beta,\varepsilon}}{\partial y^2} + \frac{1}{\varepsilon}(m-y)\frac{\partial P^{\beta,\varepsilon}}{\partial y} - rP^{\beta,\varepsilon}, \end{aligned} \tag{5}$$

valid for $x < b$ and $0 < t < T$. The terminal and boundary conditions for the up-and-out call option are as follows:

$$\begin{cases} P^{\beta,\varepsilon}(T,x,y) = \max\Big\{e^x - e^k,\, 0\Big\}, & x < b, \\ P^{\beta,\varepsilon}(t,b,y) = 0, & 0 \le t \le T. \end{cases}$$

In the next section, we will employ an asymptotic expansion technique to construct a hierarchy of partial differential equations whose solutions yield an approximation to the barrier-option price satisfying Equation (5).

3. Asymptotic Expansions

Our goal is to exploit the small-parameter structure of the SVCEV model and derive a tractable approximation for the up-and-out call option. We begin by reorganizing Equation (5) in powers of the small parameter ε:

$$\left(\frac{1}{\varepsilon}\mathcal{L}_0 + \frac{1}{\sqrt{\varepsilon}}\mathcal{L}_1^{\beta} + \mathcal{L}_2^{\beta}\right)P^{\beta,\varepsilon} = 0, \tag{6}$$

where the operators $\mathcal{L}_0$, $\mathcal{L}_1^{\beta}$, and $\mathcal{L}_2^{\beta}$ are defined by

$$\mathcal{L}_0 := (m-y)\frac{\partial}{\partial y} + \nu^2\frac{\partial^2}{\partial y^2}, \quad \mathcal{L}_1^{\beta},:= \sqrt{2}\rho\nu\, e^{\beta x} f(y)\frac{\partial^2}{\partial x\,\partial y}, \quad \mathcal{L}_2^{\beta} := \frac{\partial}{\partial t} + \tfrac{1}{2}e^{2\beta x} f^2(y)\frac{\partial^2}{\partial x^2} + \Big(r - \tfrac{1}{2}f^2(y)\Big)\frac{\partial}{\partial x} - r.$$

Next, we expand the β-dependence of both $\mathcal{L}_1^{\beta}$ and $\mathcal{L}_2^{\beta}$ by using the Taylor series expansion of $e^{\beta x}$ and $e^{2\beta x}$:

$$\mathcal{L}_1^{\beta} = \mathcal{L}_{10} + \beta\,\mathcal{L}_{11} + \beta^2\mathcal{L}_{12} + O(\beta^3) \quad \text{and} \quad \mathcal{L}_2^{\beta} = \mathcal{L}_{20} + \beta\,\mathcal{L}_{21} + \beta^2\mathcal{L}_{22} + O(\beta^3). \tag{7}$$

https://doi.org/10.3390/math14101651

The individual operators are given by

$$\mathcal{L}_{10} := \sqrt{2}\rho\nu\, f(y)\frac{\partial^2}{\partial x\,\partial y}, \quad \mathcal{L}_{11} := \sqrt{2}\rho\nu\, x f(y)\frac{\partial^2}{\partial x\,\partial y}, \quad \mathcal{L}_{12} := \tfrac{\sqrt{2}}{2}\rho\nu\, x^2 f(y)\frac{\partial^2}{\partial x\,\partial y},$$

and

$$\mathcal{L}_{20} := \frac{\partial}{\partial t} + \tfrac{1}{2}f^2(y)\frac{\partial^2}{\partial x^2} + \left(r - \tfrac{1}{2}f^2(y)\right)\frac{\partial}{\partial x} - r,$$
$$\mathcal{L}_{21} := x f^2(y)\,\frac{\partial^2}{\partial x^2}, \quad \mathcal{L}_{22} := x^2 f^2(y)\,\frac{\partial^2}{\partial x^2}.$$

To derive an efficient approximation for $P^{\beta,\varepsilon}$, following the methodology in [19], we introduce the expansion

$$P^{\beta,\varepsilon} = P_0^\varepsilon + \beta P_1^\varepsilon + \beta^2 P_2^\varepsilon + \cdots, \tag{8}$$

where each function P_j^ε corresponds to the jth-order term in β. Substituting Equations (7) and (8) into Equation (6) and collecting like powers of β yield

$$\begin{aligned} 0 &= \left(\frac{1}{\varepsilon}\mathcal{L}_0 + \frac{1}{\sqrt{\varepsilon}}\mathcal{L}_1^\beta + \mathcal{L}_2^\beta\right)\left(P_0^\varepsilon + \beta P_1^\varepsilon + \beta^2 P_2^\varepsilon + \cdots\right) \\ &= \left(\frac{1}{\varepsilon}\mathcal{L}_0 + \frac{1}{\sqrt{\varepsilon}}\mathcal{L}_{10} + \mathcal{L}_{20}\right)P_0^\varepsilon + \beta\left[\left(\frac{1}{\varepsilon}\mathcal{L}_0 + \frac{1}{\sqrt{\varepsilon}}\mathcal{L}_{10} + \mathcal{L}_{20}\right)P_1^\varepsilon + \left(\frac{1}{\sqrt{\varepsilon}}\mathcal{L}_{11} + \mathcal{L}_{21}\right)P_0^\varepsilon\right] \\ &\quad + \beta^2\left[\left(\frac{1}{\varepsilon}\mathcal{L}_0 + \frac{1}{\sqrt{\varepsilon}}\mathcal{L}_{10} + \mathcal{L}_{20}\right)P_2^\varepsilon + \left(\frac{1}{\sqrt{\varepsilon}}\mathcal{L}_{11} + \mathcal{L}_{21}\right)P_1^\varepsilon + \left(\frac{1}{\sqrt{\varepsilon}}\mathcal{L}_{12} + \mathcal{L}_{22}\right)P_0^\varepsilon\right] + O(\beta^3). \end{aligned} \tag{9}$$

3.1. The Zero-Order Term

In this subsection, we derive an analytical expression of the zero-order term (also called the leading term) $P_{0,0}$. From the $O(1)$ term in β obtained in Equation (9), the leading-order approximation P_0^ε satisfies

$$\left(\frac{1}{\varepsilon}\,\mathcal{L}_0 + \frac{1}{\sqrt{\varepsilon}}\,\mathcal{L}_{10} + \mathcal{L}_{20}\right)P_0^\varepsilon = 0. \tag{10}$$

We use the regular expansion

$$P_0^\varepsilon = P_{0,0} + \sqrt{\varepsilon}\,P_{0,1} + \varepsilon P_{0,2} + \varepsilon^{3/2}P_{0,3} + \cdots, \tag{11}$$

which leads to the recursive relation

$$\mathcal{L}_0 P_{0,k} + \mathcal{L}_{10}P_{0,k-1} + \mathcal{L}_{20}P_{0,k-2} = 0, \qquad k = 0, 1, 2, \ldots, \tag{12}$$

with $P_{0,-2} = P_{0,-1} = 0$. The first member of the hierarchy (12) is $\mathcal{L}_0 P_{0,0} = 0$. Under the standard growth condition that $P_{0,0}$ grows slower than $\exp(y^2/2)$ as $|y| \to \infty$, the only admissible solution is independent of y. The next member of the hierarchy (12) is $\mathcal{L}_{10}P_{0,0} + \mathcal{L}_0 P_{0,1} = 0$. Since $P_{0,0}$ is independent of y, $\mathcal{L}_{10}P_{0,0} = 0$, and therefore $\mathcal{L}_0 P_{0,1} = 0$. Imposing the same growth condition again implies that $P_{0,1}$ is also independent of y.

Proceeding to the next member of the hierarchy (12), we obtain $\mathcal{L}_0 P_{0,2} + \mathcal{L}_{10}P_{0,1} + \mathcal{L}_{20}P_{0,0} = 0$. Because $P_{0,1}$ is independent of y, $\mathcal{L}_{10}P_{0,1} = 0$, and the equation simplifies to

$$\mathcal{L}_0 P_{0,2} + \mathcal{L}_{20}P_{0,0} = 0. \tag{13}$$

Interpreting Equation (13) as a Poisson equation in the y-variable, a solvability (centering) condition required is as follows: $\langle \mathcal{L}_{20} P_{0,0} \rangle = \langle \mathcal{L}_{20} \rangle P_{0,0} = 0$, which yields the effective (in t, x) PDE

$$\frac{\partial P_{0,0}}{\partial t} + \frac{1}{2} \langle f^2 \rangle \frac{\partial^2 P_{0,0}}{\partial x^2} + \left(r - \tfrac{1}{2} \langle f^2 \rangle \right) \frac{\partial P_{0,0}}{\partial x} - r P_{0,0} = 0, \qquad (t, x) \in [0, T) \times (-\infty, b), \quad (14)$$

with boundary and terminal conditions:

$$P_{0,0}(T, x) = \max(e^x - e^k, 0),\ x < b, \quad \text{and} \quad P_{0,0}(t, b) = 0,\ 0 \le t \le T.$$

Here, the averaging operator $\langle \cdot \rangle$ with respect to the invariant distribution of the process $\{Y_t\}$ is defined by the following equation:

$$\langle h \rangle := \int_{-\infty}^{\infty} h(y)\, \pi(y)\, dy, \qquad \pi(y) = \frac{1}{\sqrt{2\pi\nu^2}} \exp\left(-\frac{(y-m)^2}{2\nu^2} \right),$$

where π is the density of the invariant distribution of $\{Y_t : t \ge 0\}$. Because $\langle f^2 \rangle$ is a constant, Equation (14) is the classical Black–Scholes PDE with effective volatility $\sqrt{\langle f^2 \rangle}$. Thus, for a small ε, the leading approximation term $P_{0,0}$ is the Black–Scholes price of an up-and-out call option.

To derive an analytical expression for $P_{0,0}$, we first consider the following auxiliary problem for $Q_{0,0}$:

$$\begin{aligned} &\frac{\partial Q_{0,0}}{\partial t} + \frac{1}{2} \langle f^2 \rangle \frac{\partial^2 Q_{0,0}}{\partial x^2} + \left(r - \frac{1}{2} \langle f^2 \rangle \right) \frac{\partial Q_{0,0}}{\partial x} - r\, Q_{0,0} = 0, \\ &Q_{0,0}(T, x) = h(x) := (e^x - e^k)^+\, u(b - x), \end{aligned} \qquad (15)$$

where $u(\cdot)$ is the Heaviside function. This corresponds to a "low-pass" (below-barrier) payout at expiry. The difference between (14) and (15) lies in the domain restriction and the boundary condition at $x = b$. By the method of images,

$$P_{0,0}(t, x) = Q_{0,0}(t, x) - Q^*_{0,0}(t, x), \qquad (16)$$

where $Q^*_{0,0}$ solves the same PDE as $Q_{0,0}$ but with a different terminal condition:

$$\begin{aligned} &\frac{\partial Q^*_{0,0}}{\partial t} + \frac{1}{2} \langle f^2 \rangle \frac{\partial^2 Q^*_{0,0}}{\partial x^2} + \left(r - \frac{1}{2} \langle f^2 \rangle \right) \frac{\partial Q^*_{0,0}}{\partial x} - r\, Q^*_{0,0} = 0, \\ &Q^*_{0,0}(T, x) = h^*(x) := e^{(b-x)(k_1-1)} (e^{2b-x} - e^k)^+ u(x - b), \end{aligned} \qquad (17)$$

where $k_1 := \dfrac{2r}{\langle f^2 \rangle}$.

We now utilize the (generalized) Fourier transform method to solve Equation (15). Recall that Fourier transform and its inverse transform are defined by

$$(\mathcal{F} f)(\theta) = \hat{f}(\theta) := \frac{1}{\sqrt{2\pi}} \int_{\mathbb{R}} f(x)\, e^{-i\theta x}\, dx, \qquad (\mathcal{F}^{-1} g)(x) := \frac{1}{\sqrt{2\pi}} \int_{\mathbb{R}} g(\theta)\, e^{i\theta x}\, d\theta.$$

Define the *phi*-function φ by

$$\varphi(\theta) := \left(r - \frac{1}{2} \langle f^2 \rangle \right) i\theta - \frac{1}{2} \langle f^2 \rangle \theta^2 - r. \qquad (18)$$

This symbol will represent the Fourier multiplier of the spatial operator in (15).

Proposition 1. *The solution to Equation (15) is given by*

$$Q_{0,0}(t,x) = e^x\,\Phi(-d_3) + e^{k-r(T-t)}\,\Phi(d_4) - e^x\,\Phi(-d_1) - e^{k-r(T-t)}\,\Phi(d_2), \tag{19}$$

where Φ denotes the CDF of the standard normal distribution, and d_i's ($1 \le i \le 4$) are given by

$$d_1 = \frac{x-k+(r+\frac{1}{2}\langle f^2\rangle)(T-t)}{\sqrt{\langle f^2\rangle(T-t)}},\ d_2 = d_1 - \sqrt{\langle f^2\rangle(T-t)},$$

$$d_3 = \frac{x-b+(r+\frac{1}{2}\langle f^2\rangle)(T-t)}{\sqrt{\langle f^2\rangle(T-t)}},\ d_4 = d_3 - \sqrt{\langle f^2\rangle(T-t)}.$$

Proof. Performing Fourier transform on Equation (15) in x gives

$$\partial_t \hat{Q}_{0,0}(t,\theta) = -\varphi(\theta)\,\hat{Q}_{0,0}(t,\theta), \quad \hat{Q}_{0,0}(T,\theta) = \hat{h}(\theta),$$

and hence $\hat{Q}_{0,0}(t,\theta) = e^{(T-t)\,\varphi(\theta)}\,\hat{h}(\theta)$. Applying inverse Fourier transform, we obtain

$$Q_{0,0}(t,x) = \frac{1}{\sqrt{2\pi}}\int_{\mathbb{R}} e^{\varphi(\theta)(T-t)}\,\hat{h}(\theta)\,e^{i\theta x}\,d\theta. \tag{20}$$

For $h(x) = (e^x - e^k)^+\,u(b-x)$ we have

$$\begin{aligned}\hat{h}(\theta) &= \frac{1}{\sqrt{2\pi}}\int_{\mathbb{R}} (e^x - e^k)^+ u(b-x)\,e^{-i\theta x}\,dx = \frac{1}{\sqrt{2\pi}}\int_k^b (e^x - e^k)\,e^{-i\theta x}\,dx \\ &= \frac{1}{\sqrt{2\pi}}\left(\frac{e^{b(1-i\theta)} - e^{k(1-i\theta)}}{1-i\theta} - \frac{e^{k(1-i\theta)} - e^{k(1-i\theta)}\,e^{-i\theta(k-b)}}{-i\theta}\right) \\ &= \frac{1}{\sqrt{2\pi}}\left(\frac{e^{b-i\theta b}}{1-i\theta} - \frac{e^{k-i\theta b}}{-i\theta} - \frac{e^{k-i\theta k}}{1-i\theta} + \frac{e^{k-i\theta k}}{-i\theta}\right).\end{aligned} \tag{21}$$

For $n > 0$, we will use the following identities (whose proofs are provided in the Appendix A):

$$\frac{1}{2\pi}\int_{-\infty}^{\infty} \frac{1}{i\theta}\,\exp\left(-\frac{1}{2}n\theta^2 + im\theta\right)d\theta = \Phi\left(\frac{m}{\sqrt{n}}\right) - \frac{1}{2}, \tag{22}$$

$$\frac{1}{2\pi}\int_{-\infty}^{\infty} \frac{1}{1-i\theta}\,\exp\left(-\frac{1}{2}n\theta^2 + im\theta\right)d\theta = \exp\left(m+\tfrac{1}{2}n\right)\Phi\left(-\frac{m+n}{\sqrt{n}}\right). \tag{23}$$

Inserting (21) into (20) and then evaluating it by using (22) and (23) yield Equation (19). □

Now we can apply Proposition 1 to derive an analytical formula for $P_{0,0}$.

Corollary 1. *The zero-order term $P_{0,0}$ is given by the following formula*

$$P_{0,0}(t,x) = Q_{0,0}(t,x) - e^{(k_1-1)(b-x)}\,Q_{0,0}(t,2b-x), \tag{24}$$

where $Q_{0,0}$ is given by Equation (19).

Proof. Applying Proposition 1 to Equation (17) gives an expression of $Q^*_{0,0}$ as

$$Q^*_{0,0}(t,x) = e^{(k_1-1)(b-x)}\,Q_{0,0}(t,2b-x). \tag{25}$$

Now, plugging $Q^*_{0,0}$ in Equation (25) into Equation (16) yields the formula in Equation (24). □

Please note that the analytical expression of $P_{0,0}$ in Equation (24) matches the classic up-and-out call price with volatility $\sqrt{\langle f^2 \rangle}$; see, e.g., [22] (Ch. 26) or [23] (Ch. 4). Furthermore, as $b \to \infty$, the image term vanishes and $P_{0,0}$ reduces to the vanilla Black–Scholes call. As $t \to T$, $P_{0,0}(t,x) \to (e^x - e^k)^+$ for $x < b$ and $P_{0,0}(t,b) = 0$.

3.2. The Correction Terms

In this subsection, we determine the first-order correction terms. First, note that Equation (13) identifies $P_{0,2}$ by solving a Poisson equation in the variable y: $\mathcal{L}_0 P_{0,2} = -\mathcal{L}_{20} P_{0,0}$. Then, the solvability of this equation yields $\langle \mathcal{L}_{20} P_{0,0} \rangle = 0$. Since $\mathcal{L}_0$ is the generator of an ergodic Markov process with invariant density π in y, then $P_{0,2} = \mathcal{L}_0^{-1}(-\mathcal{L}_{20} P_{0,0})$, where $\mathcal{L}_0^{-1}$ denotes the pseudo-inverse of $\mathcal{L}_0$ acting on the centered function. The same procedure yields $P_{0,3}, P_{0,4}, \ldots$ from the hierarchy (12), with a centering (solvability) condition imposed at each step to ensure the existence of a solution.

At $k = 1$ the equation reads $\mathcal{L}_0 P_{0,1} + \mathcal{L}_{10} P_{0,0} = 0$, and since $P_{0,0}$ is y-independent we have $\mathcal{L}_{10} P_{0,0} = 0$. Consequently, $\mathcal{L}_0 P_{0,1} = 0$. With the usual growth condition in y and homogeneous terminal/boundary conditions for the correctors, it follows that $P_{0,1}$ is independent of y and thus identically zero.

For $k = 3$, from $\mathcal{L}_{20} P_{0,1} + \mathcal{L}_0 P_{0,3} = 0$ and $P_{0,1} \equiv 0$, we conclude that $\mathcal{L}_0 P_{0,3} = 0$. So, $P_{0,3} \equiv 0$ under the same boundary/terminal conditions. By repeating this argument, one obtains that

$$P_{0,2j+1} \equiv 0, \qquad j = 0, 1, 2, \ldots, \tag{26}$$

whereas the even-order terms $P_{0,2j}$ are determined by Poisson problems.

3.2.1. First-Order Correction Term $P_{1,0}$

From the $O(\beta)$ contribution in (9), we have

$$\left(\frac{1}{\varepsilon} \mathcal{L}_0 + \frac{1}{\sqrt{\varepsilon}} \mathcal{L}_{10} + \mathcal{L}_{20} \right) P_1^\varepsilon + \left(\frac{1}{\sqrt{\varepsilon}} \mathcal{L}_{11} + \mathcal{L}_{21} \right) P_0^\varepsilon = 0. \tag{27}$$

Next, we introduce the regular expansion

$$P_1^\varepsilon = P_{1,0} + \sqrt{\varepsilon}\, P_{1,1} + \varepsilon\, P_{1,2} + \varepsilon^{3/2} P_{1,3} + \cdots,$$

and substitute P_1^ε into (27) to obtain the sequence of equations by matching powers of ε:

$$\begin{aligned} 0 = {} & \frac{1}{\varepsilon} \mathcal{L}_0 P_{1,0} + \frac{1}{\sqrt{\varepsilon}} \Big(\mathcal{L}_0 P_{1,1} + \mathcal{L}_{10} P_{1,0} + \mathcal{L}_{11} P_{0,0} \Big) + \Big(\mathcal{L}_0 P_{1,2} + \mathcal{L}_{10} P_{1,1} + \mathcal{L}_{20} P_{1,0} + \mathcal{L}_{21} P_{0,0} \Big) \\ & + \sqrt{\varepsilon} \Big(\mathcal{L}_0 P_{1,3} + \mathcal{L}_{10} P_{1,2} + \mathcal{L}_{20} P_{1,1} \Big) + O(\varepsilon). \end{aligned} \tag{28}$$

From the leading $O(\varepsilon^{-1})$ term in Equation (28), we get $\mathcal{L}_0 P_{1,0} = 0$. Under a growth condition in y like that used on $P_{0,0}$, $P_{1,0}$ is y-independent. Moreover, from the $O(\varepsilon^{-1/2})$ term in Equation (28), we obtain $\mathcal{L}_0 P_{1,1} + \mathcal{L}_{10} P_{1,0} + \mathcal{L}_{11} P_{0,0} = 0$. Since $P_{1,0}$ and $P_{0,0}$ are y-independent, $\mathcal{L}_{10} P_{1,0} = 0$ and (in the common multiscale setups) $\mathcal{L}_{11} P_{0,0}$ is centered in y, which leaves $\mathcal{L}_0 P_{1,1} = 0$, hence $P_{1,1}$ is y-independent as well.

From the $O(1)$ term in Equation (28), we obtain $\mathcal{L}_0 P_{1,2} + \mathcal{L}_{20} P_{1,0} + \mathcal{L}_{21} P_{0,0} = 0$. A solvability (centering) condition ensuring the existence of a solution for $P_{1,2}$ yields $\langle \mathcal{L}_{20} P_{1,0} + \mathcal{L}_{21} P_{0,0} \rangle = \langle \mathcal{L}_{20} \rangle P_{1,0} + \langle \mathcal{L}_{21} \rangle P_{0,0} = 0$. This produces the following PDE for $P_{1,0}(t,x)$ (the y-averaged first-order corrector):

$$\begin{aligned} & \frac{\partial P_{1,0}}{\partial t} + \frac{1}{2} \langle f^2 \rangle \frac{\partial^2 P_{1,0}}{\partial x^2} + \Big(r - \tfrac{1}{2} \langle f^2 \rangle \Big) \frac{\partial P_{1,0}}{\partial x} - r\, P_{1,0} = x \langle f^2 \rangle \frac{\partial^2 P_{0,0}}{\partial x^2} \\ & (t,x) \in [0,T) \times (-\infty, b), \end{aligned} \tag{29}$$

with boundary and terminal conditions:

$$P_{1,0}(T,x) = 0,\ x < b, \quad \text{and} \quad P_{1,0}(t,b) = 0,\ 0 \le t \le T.$$

To proceed forward, as we have done for $P_{0,0}$, we split $P_{1,0}(t,x)$ as $P_{1,0}(t,x) = Q_{1,0}(t,x) - Q^*_{1,0}(t,x)$, where $Q_{1,0}$ solves the inhomogeneous PDE without a barrier:

$$\begin{cases} \dfrac{\partial Q_{1,0}}{\partial t} + \dfrac{1}{2}\langle f^2\rangle \dfrac{\partial^2 Q_{1,0}}{\partial x^2} + \left(r - \frac{1}{2}\langle f^2\rangle\right)\dfrac{\partial Q_{1,0}}{\partial x} - r\,Q_{1,0} = x\,\langle f^2\rangle \dfrac{\partial^2 \tilde{Q}_{0,0}}{\partial x^2}, \\ Q_{1,0}(T,x) = 0, \end{cases} \tag{30}$$

with $\tilde{Q}_{0,0}(t,x) := Q_{0,0}(t,x)\,\mathbf{1}_{\{x<b\}}$. The image term $Q^*_{1,0}$ solves the PDE

$$\begin{cases} \dfrac{\partial Q^*_{1,0}}{\partial t} + \dfrac{1}{2}\langle f^2\rangle \dfrac{\partial^2 Q^*_{1,0}}{\partial x^2} + \left(r - \frac{1}{2}\langle f^2\rangle\right)\dfrac{\partial Q^*_{1,0}}{\partial x} - r\,Q^*_{1,0} = x\,\langle f^2\rangle \dfrac{\partial^2 \tilde{Q}^*_{0,0}}{\partial x^2}, \\ Q^*_{1,0}(T,x) = 0, \end{cases} \tag{31}$$

with $\tilde{Q}^*_{0,0}(t,x) := Q^*_{0,0}(t,x)\,\mathbf{1}_{\{x>b\}}$. Note that $Q^*_{1,0}$ can be written explicitly once $Q_{1,0}$ is known:

$$Q^*_{1,0}(t,x) = e^{(k_1-1)(b-x)}\,Q_{1,0}(t,2b-x), \qquad \text{where} \quad k_1 := \frac{2r}{\langle f^2\rangle}, \tag{32}$$

which satisfies the boundary matching at $x = b$.

Proposition 2. *With $\varphi(\theta)$ given in Equation (18) and $\hat{h}$, the Fourier transform of the (truncated) call payoff in Equation (21), $Q_{1,0}$, can be expressed as*

$$Q_{1,0}(t,x) = \frac{1}{\sqrt{2\pi}}\int_{\mathbb{R}} e^{(T-t)\varphi(\theta)}\,H_{10}(t,\theta)\,e^{i\theta x}\,d\theta, \tag{33}$$

where

$$H_{10}(t,\theta) := \langle f^2\rangle\,(T-t)\left(\hat{h}'(\theta)\,i\theta^2 + 2\,\hat{h}(\theta)\,i\theta\right) + \frac{1}{2}\langle f^2\rangle\,(T-t)^2\,\hat{h}(\theta)\,i\theta^2\,\frac{\partial\varphi(\theta)}{\partial\theta}.$$

Hence, the first-order correction term $P_{1,0}$ is then given by

$$P_{1,0}(t,x) = Q_{1,0}(t,x) - e^{(k_1-1)(b-x)}\,Q_{1,0}(t,2b-x), \qquad \text{where} \quad k_1 = \frac{2r}{\langle f^2\rangle}. \tag{34}$$

Proof. Define the source

$$R_{1,0}(t,x) := x\,\langle f^2\rangle\,\frac{\partial^2 \tilde{Q}_{0,0}(t,x)}{\partial x^2},$$

with the Fourier conventional notation

$$\hat{f}(\theta) = \frac{1}{\sqrt{2\pi}}\int_{\mathbb{R}} f(x)e^{-i\theta x}dx, \qquad f(x) = \frac{1}{\sqrt{2\pi}}\int_{\mathbb{R}} \hat{f}(\theta)e^{i\theta x}d\theta,$$

and the symbol ("phi function")

$$\varphi(\theta) := \left(r - \tfrac{1}{2}\sigma^2\right)i\theta - \tfrac{1}{2}\sigma^2\theta^2 - r, \qquad \partial_\theta\varphi(\theta) = i\left(r - \tfrac{1}{2}\sigma^2\right) - \sigma^2\theta,$$

we obtain the following using the Duhamel formula

$$\hat{Q}_{1,0}(t,\theta) = -\int_t^T e^{(s-t)\varphi(\theta)}\,\widehat{R}_{1,0}(s,\theta)\,ds. \tag{35}$$

Using $Q_{0,0}(t,x) = \frac{1}{\sqrt{2\pi}} \int e^{(T-t)\varphi(\tilde{\theta})} \hat{h}(\tilde{\theta})\, e^{i\tilde{\theta}x} d\tilde{\theta}$ (from Proposition 1), we compute

$$R_{1,0}(t,x) = x\,\langle f^2\rangle\,\frac{\partial^2 \tilde{Q}_{0,0}(t,x)}{\partial x^2} = -\frac{\langle f^2\rangle}{\sqrt{2\pi}} \int_{\mathbb{R}} \hat{h}(\tilde{\theta})\, e^{(T-t)\varphi(\tilde{\theta})}\, \tilde{\theta}^2\, x\, e^{i\tilde{\theta}x}\, d\tilde{\theta}.$$

Hence, by Fubini and distributional calculus (with $\int_{\mathbb{R}} x e^{ikx} dx = -2\pi i\, \delta'(k)$),

$$\begin{aligned}
\widehat{R}_{1,0}(t,\theta) &= -\frac{\langle f^2\rangle}{2\pi} \int_{\mathbb{R}}\int_{\mathbb{R}} \hat{h}(\tilde{\theta})\, e^{(T-t)\varphi(\tilde{\theta})}\, \tilde{\theta}^2\, x\, e^{i(\tilde{\theta}-\theta)x}\, dx\, d\tilde{\theta} \\
&= \langle f^2\rangle \int_{\mathbb{R}} \hat{h}(\tilde{\theta})\, e^{(T-t)\varphi(\tilde{\theta})}\, i\tilde{\theta}^2\, \delta'(\tilde{\theta}-\theta)\, d\tilde{\theta} \\
&= -\langle f^2\rangle \frac{\partial}{\partial\theta}\Big(\hat{h}(\theta)\, e^{(T-t)\varphi(\theta)}\, i\theta^2\Big) \\
&= -\langle f^2\rangle \Big(\hat{h}'(\theta)\, e^{(T-t)\varphi(\theta)}\, i\theta^2 + (T-t)\,\frac{\partial\varphi(\theta)}{\partial\theta}\,\hat{h}(\theta)\, e^{(T-t)\varphi(\theta)}\, i\theta^2 + 2\,\hat{h}(\theta)\, e^{(T-t)\varphi(\theta)}\, i\theta\Big).
\end{aligned} \tag{36}$$

Substituting (36) into (35) and integrating in s yields

$$\begin{aligned}
\hat{Q}_{1,0}(t,\theta) &= \langle f^2\rangle\,(T-t)\,\Big(\hat{h}'(\theta)\, i\theta^2 + 2\,\hat{h}(\theta)\, i\theta\Big)\, e^{(T-t)\varphi(\theta)} \\
&+\frac{1}{2}\langle f^2\rangle\,(T-t)^2\,\hat{h}(\theta)\, i\theta^2\,\frac{\partial\varphi(\theta)}{\partial\theta}\, e^{(T-t)\varphi(\theta)}.
\end{aligned} \tag{37}$$

Taking the inverse transform gives the expression of $Q_{1,0}(t,x)$ in Equation (33). □

3.2.2. First-Order Correction Term $P_{1,1}$

Next, we find a solution for $P_{1,1}$. From the $O(\sqrt{\varepsilon})$ terms, we get $\mathcal{L}_{20}P_{1,1} + \mathcal{L}_{10}P_{1,2} + \mathcal{L}_0 P_{1,3} = 0$. The existence of a solution for $P_{1,3}$ requires $\mathcal{L}_{20}P_{1,1} + \langle \mathcal{L}_{10}P_{1,2}\rangle = 0$. By solving $\mathcal{L}_0 P_{1,2} = (\langle\mathcal{L}_{21}\rangle - \mathcal{L}_{21})P_{0,0}$, we obtain

$$P_{1,2} = x\frac{\partial^2 P_{0,0}}{\partial x^2}\mathcal{L}_0^{-1}\Big(f^2 - \big\langle f^2\big\rangle\Big).$$

Then, we can obtain the solution for $P_{1,1}$ by solving the equation

$$\begin{aligned}
\mathcal{L}_{20}P_{1,1} &= -\langle\mathcal{L}_{10}P_{1,2}\rangle = -\sqrt{2}\rho v\big\langle f\psi'\big\rangle\frac{\partial}{\partial x}\left(x\frac{\partial^2 P_{0,0}}{\partial x^2}\right), \\
P_{1,1}(T,s) &= 0, \quad P_{1,1}(t,B) = 0,
\end{aligned} \tag{38}$$

where ψ is the solution of $\mathcal{L}_0\psi = f^2 - \langle f^2\rangle$. As for $P_{1,0}$, we split $P_{1,1}$ as $P_{1,1}(t,x) = Q_{1,1}(t,x) - Q^*_{1,1}(t,x)$, where $Q_{1,1}$ solves the following inhomogeneous PDE:

$$\begin{cases}
\frac{\partial Q_{1,1}}{\partial t} + \frac{1}{2}\langle f^2\rangle\frac{\partial^2 Q_{1,1}}{\partial x^2} + \Big(r - \frac{1}{2}\langle f^2\rangle\Big)\frac{\partial Q_{1,1}}{\partial x} - r\,Q_{1,1} = -\sqrt{2}\rho v\big\langle f\psi'\big\rangle\frac{\partial}{\partial x}\left(x\frac{\partial^2\tilde{Q}_{0,0}}{\partial x^2}\right), \\
Q_{1,1}(T,x) = 0,
\end{cases} \tag{39}$$

with $\tilde{Q}_{0,0}(t,x) := Q_{0,0}(t,x)\,\mathbf{1}_{\{x<b\}}$. The image term $Q^*_{1,1}$ solves the PDE

$$\begin{cases}
\frac{\partial Q^*_{1,1}}{\partial t} + \frac{1}{2}\langle f^2\rangle\frac{\partial^2 Q^*_{1,1}}{\partial x^2} + \Big(r - \frac{1}{2}\langle f^2\rangle\Big)\frac{\partial Q^*_{1,1}}{\partial x} - r\,Q^*_{1,1} = -\sqrt{2}\rho v\big\langle f\psi'\big\rangle\frac{\partial}{\partial x}\left(x\frac{\partial^2\tilde{Q}^*_{0,0}}{\partial x^2}\right), \\
Q^*_{1,1}(T,x) = 0,
\end{cases} \tag{40}$$

with $\tilde{Q}^*_{0,0}(t,x) := Q^*_{0,0}(t,x)\,\mathbf{1}_{\{x>b\}}$. Note that $Q^*_{1,1}$ can be written explicitly once $Q_{1,1}$ is known:

$$Q^*_{1,1}(t,x) = e^{(k_1-1)(b-x)}\,Q_{1,1}(t,2b-x), \qquad \text{with} \quad k_1 := \frac{2r}{\langle f^2\rangle}, \tag{41}$$

which satisfies the boundary matching at $x = b$.

Proposition 3. *With $\varphi(\theta)$ given in Equation (18) and $\hat{h}$ the Fourier transform of the (truncated) call payoff in (21), $Q_{1,1}(t,x)$ can be expressed as*

$$Q_{1,1}(t,x) = \frac{1}{\sqrt{2\pi}} \int_{\mathbb{R}} H_{11}(t,\theta)\, e^{i\theta x}\, d\theta, \tag{42}$$

where

$$\begin{aligned} H_{11}(t,\theta) &= \sqrt{2}\rho v \langle f\psi' \rangle \theta^2 \int_t^T e^{(s-t)\varphi(\theta)} \hat{Q}_{0,0}(s,\theta), ds + \sqrt{2}\rho v \langle f\psi' \rangle \Big((T-t)\hat{h}'(\theta)\, e^{(T-t)\varphi(\theta)}\, \theta^3 \\ &\quad + \frac{(T-t)^2}{2} \frac{\partial \varphi}{\partial \theta} \hat{h}(\theta)\, e^{(T-t)\varphi(\theta)}\, \theta^3 + 3(T-t)\, \hat{h}(\theta)\, e^{(T-t)\varphi(\theta)}\, \theta^2 \Big) \end{aligned}$$

Hence, the first-order correction term $P_{1,1}$ is then given by

$$P_{1,1}(t,x) = Q_{1,1}(t,x) - e^{(k_1-1)(b-x)}\, Q_{1,1}(t, 2b-x), \qquad \text{with} \quad k_1 = \frac{2r}{\langle f^2 \rangle}. \tag{43}$$

Proof. To obtain a solution for the PDE for $Q_{1,1}(t,x)$, we use the notation

$$R_{1,1}(t,x) := -\sqrt{2}\rho v \langle f\psi' \rangle (\partial_{xx} Q_{0,0} + x \partial_{xxx} Q_{0,0}) + \sqrt{2} v \langle \Lambda \psi' \rangle x \partial_{xx} Q_{0,0}.$$

The Duhamel formula gives

$$\hat{Q}_{1,1}(t,\theta) = -\int_t^T e^{(s-t)\varphi(\theta)}\, \hat{R}_{1,1}(s,\theta)\, ds, \tag{44}$$

where $\hat{Q}_{1,1}$ and $\hat{R}_{1,1}$ are the Fourier transformation of $Q_{1,1}$ and $R_{1,1}$. Using the formula $Q_{0,0}(t,x) = \frac{1}{\sqrt{2\pi}} \int e^{(T-t)\varphi(\tilde{\theta})} \hat{h}(\tilde{\theta})\, e^{i\tilde{\theta}x} d\tilde{\theta}$, we compute that

$$\begin{aligned} & R_{1,1}(t,x) \\ = \;& -\sqrt{2}\rho v \langle f\psi' \rangle (\partial_{xx} Q_{0,0} + x \partial_{xxx} Q_{0,0}) + \sqrt{2} v \langle \Lambda \psi' \rangle x \partial_{xx} Q_{0,0} \\ = \;& -\sqrt{2}\rho v \langle f\psi' \rangle \left(\frac{-1}{\sqrt{2\pi}} \int_{\mathbb{R}} \hat{h}(\tilde{\theta})\, e^{(T-t)\varphi(\tilde{\theta})}\, \tilde{\theta}^2\, e^{i\tilde{\theta}x}\, d\tilde{\theta} - \frac{i}{\sqrt{2\pi}} \int_{\mathbb{R}} \hat{h}(\tilde{\theta})\, e^{(T-t)\varphi(\tilde{\theta})}\, \tilde{\theta}^3\, x\, e^{i\tilde{\theta}x}\, d\tilde{\theta} \right) \\ & -\sqrt{2} v \langle \Lambda \psi' \rangle \frac{1}{\sqrt{2\pi}} \int_{\mathbb{R}} \hat{h}(\tilde{\theta})\, e^{(T-t)\varphi(\tilde{\theta})}\, \tilde{\theta}^2\, x\, e^{i\tilde{\theta}x}\, d\tilde{\theta} \end{aligned}$$

Hence, by Fubini and distributional calculus (with $\int_{\mathbb{R}} x e^{ikx} dx = -2\pi i\, \delta'(k)$),

$$\begin{aligned} & \hat{R}_{1,1}(t,\theta) \\ =& \sqrt{2}\rho v \langle f\psi' \rangle \frac{1}{2\pi} \int_{\mathbb{R}}\int_{\mathbb{R}} \hat{h}(\tilde{\theta})\, e^{(T-t)\varphi(\tilde{\theta})}\, \tilde{\theta}^2\, e^{i(\tilde{\theta}-\theta)x}\, dx\, d\tilde{\theta} \\ & + \sqrt{2}\rho v \langle f\psi' \rangle \frac{i}{2\pi} \int_{\mathbb{R}}\int_{\mathbb{R}} \hat{h}(\tilde{\theta})\, e^{(T-t)\varphi(\tilde{\theta})}\, \tilde{\theta}^3\, x\, e^{i(\tilde{\theta}-\theta)x}\, dx\, d\tilde{\theta} \\ & - \sqrt{2} v \langle \Lambda \psi' \rangle \frac{1}{2\pi} \int_{\mathbb{R}}\int_{\mathbb{R}} \hat{h}(\tilde{\theta})\, e^{(T-t)\varphi(\tilde{\theta})}\, \tilde{\theta}^2\, x\, e^{i(\tilde{\theta}-\theta)x}\, dx\, d\tilde{\theta} \\ & = -\sqrt{2}\rho v \langle f\psi' \rangle \theta^2 \hat{Q}_{0,0} \\ & + \sqrt{2}\rho v \langle f\psi' \rangle \int_{\mathbb{R}} \hat{h}(\tilde{\theta})\, e^{(T-t)\varphi(\tilde{\theta})}\, \tilde{\theta}^3\, \delta'(\tilde{\theta}-\theta) d\tilde{\theta} \\ & + i\sqrt{2} v \langle \Lambda \psi' \rangle \int_{\mathbb{R}} \hat{h}(\tilde{\theta})\, e^{(T-t)\varphi(\tilde{\theta})}\, \tilde{\theta}^2\, \delta'(\tilde{\theta}-\theta) d\tilde{\theta} \\ & = -\sqrt{2}\rho v \langle f\psi' \rangle \theta^2 \hat{Q}_{0,0} \\ & - \sqrt{2}\rho v \langle f\psi' \rangle \partial_\theta \Big(\hat{h}(\theta)\, e^{(T-t)\varphi(\theta)}\, \theta^3 \Big) \\ & - i\sqrt{2} v \langle \Lambda \psi' \rangle \partial_\theta \Big(\hat{h}(\theta)\, e^{(T-t)\varphi(\theta)}\, \theta^2 \Big) \\ & = -\sqrt{2}\rho v \langle f\psi' \rangle \theta^2 \hat{Q}_{0,0} \\ & - \sqrt{2}\rho v \langle f\psi' \rangle \Big(\hat{h}'(\theta)\, e^{(T-t)\varphi(\theta)}\, \theta^3 + (T-t)\, \partial_\theta \varphi(\theta)\, \hat{h}(\theta)\, e^{(T-t)\varphi(\theta)}\, \theta^3 + 3\, \hat{h}(\theta)\, e^{(T-t)\varphi(\theta)}\, \theta^2 \Big) \\ & - i\sqrt{2} v \langle \Lambda \psi' \rangle \Big(\hat{h}'(\theta)\, e^{(T-t)\varphi(\theta)}\, \theta^2 + (T-t)\, \partial_\theta \varphi(\theta)\, \hat{h}(\theta)\, e^{(T-t)\varphi(\theta)}\, \theta^2 + 2\, \hat{h}(\theta)\, e^{(T-t)\varphi(\theta)}\, \theta \Big) \end{aligned} \tag{45}$$

Substituting (45) into (44) and integrating in s yields

$$\begin{aligned}
\hat{Q}_{1,1}(t,\theta) &= -\int_t^T e^{(s-t)\varphi(\theta)}\,\hat{R}_{1,1}(s,\theta)\,ds \\
&= \sqrt{2}\rho v\langle f\psi'\rangle\theta^2\int_t^T e^{(s-t)\varphi(\theta)}\hat{Q}_{0,0}(s,\theta),ds \\
&\quad+\sqrt{2}\rho v\langle f\psi'\rangle\int_t^T\Big(\hat{h}'(\theta)\,e^{(T-t)\varphi(\theta)}\,\theta^3+(T-s)\,\partial_\theta\varphi(\theta)\,\hat{h}(\theta)\,e^{(T-t)\varphi(\theta)}\,\theta^3 \\
&\quad+3\,\hat{h}(\theta)\,e^{(T-t)\varphi(\theta)}\,\theta^2\Big)ds \\
&\quad+i\sqrt{2}v\langle\Lambda\psi'\rangle\int_t^T\Big(\hat{h}'(\theta)\,e^{(T-t)\varphi(\theta)}\,\theta^2+(T-s)\,\partial_\theta\varphi(\theta)\,\hat{h}(\theta)\,e^{(T-t)\varphi(\theta)}\,\theta^2 \\
&\quad+2\,\hat{h}(\theta)\,e^{(T-t)\varphi(\theta)}\,\theta\Big)ds \\
&= \sqrt{2}\rho v\langle f\psi'\rangle\theta^2\int_t^T e^{(s-t)\varphi(\theta)}\hat{Q}_{0,0}(s,\theta),ds \\
&\quad+\sqrt{2}\rho v\langle f\psi'\rangle\Big((T-t)\hat{h}'(\theta)\,e^{(T-t)\varphi(\theta)}\,\theta^3+\frac{(T-t)^2}{2}\,\partial_\theta\varphi(\theta)\,\hat{h}(\theta)\,e^{(T-t)\varphi(\theta)}\,\theta^3 \\
&\quad+3(T-t)\,\hat{h}(\theta)\,e^{(T-t)\varphi(\theta)}\,\theta^2\Big) \\
&\quad+i\sqrt{2}v\langle\Lambda\psi'\rangle\Big((T-t)\hat{h}'(\theta)\,e^{(T-t)\varphi(\theta)}\,\theta^2+\frac{(T-t)^2}{2}\,\partial_\theta\varphi(\theta)\,\hat{h}(\theta)\,e^{(T-t)\varphi(\theta)}\,\theta^2 \\
&\quad+2\,(T-t)\hat{h}(\theta)\,e^{(T-t)\varphi(\theta)}\,\theta\Big)
\end{aligned}$$

Taking the inverse Fourier transform gives the expression of $Q_{1,1}(t,x)$ in Equation (42). □

Collecting the leading-order barrier price $P_{0,0}$ from (24), with the fact that all the terms $P_{0,2j+1}$ vanish, and the first-order (in β) correction $P_{1,0}$ from (34) and $P_{1,1}$ from (43), we obtain the following corollary.

Corollary 2. *The risk-neutral price $P^{\beta,\varepsilon}(t,x)$ of an up-and-out call option on a risky equity $\{S_t : t \geq 0\}$, whose price dynamics are governed by Equation (3), can be approximated by the following formula*

$$\tilde{P}^{\beta,\varepsilon}(t,x) := P_{0,0}(t,x)+\beta P_{1,0}(t,x)+\beta\sqrt{\varepsilon}\,P_{1,1}(t,x) \tag{46}$$

for small ε and β, where $P_{0,0}$, $P_{1,0}$ and $P_{1,1}$ are given by (24), (34) and (43), respectively.

Remark 1. *Following the relationship (4), the semi-closed form formula (46), put–call-parity and the pricing formula of vanilla call options in [16], we are able to work out the valuation of up-and-out put, up-and-in call, and up-and-in put options under the SVCEV model.*

4. Numerical Experiments

This section presents a numerical assessment of the asymptotic approximation derived in Corollary 2. The experiments have three main objectives. First, we evaluate the accuracy of the approximate up-and-out barrier call price by comparing it with benchmark values obtained from Monte Carlo simulation and compare the computational efficiency and relative errors among our semi-close pricing formula, Monte Carlo simulation, and the binomial tree method in [17]. Second, we examine the sensitivity of the option value to the principal perturbation parameters of the model, namely the stochastic-volatility time-scale parameter ε, the elasticity parameter β, and the long-term mean parameter m. Third, we investigate three limiting regimes to verify that the approximation is consistent with the reduced models obtained when one or more perturbative effects vanish.

Throughout this section, unless stated otherwise, we use the specification $f(y) = \sqrt{y}$, which is common in the asymptotic stochastic-volatility literature; see, for example, refs. [20,21]. This choice guarantees positivity of the instantaneous volatility whenever $Y_t > 0$ and allows for a transparent comparison with familiar stochastic-volatility benchmark models. In particular, the map $y \mapsto \sqrt{y}$ gives a direct interpretation of Y_t as an instantaneous variance factor, which is convenient both analytically and numerically.

The baseline parameter values used throughout the numerical study are reported in Table 1. They are chosen so that the option is neither nearly worthless nor close to immediate knock-out. In particular, the barrier is placed sufficiently above the initial spot price to ensure that the barrier feature has a material, but non-degenerate, effect on the option value. At the same time, the perturbation parameters are kept within a range consistent with the asymptotic assumptions underlying the approximation.

Table 1. Baseline parameter values used in the numerical experiments.

Parameter	K	B	r	S_0	Y_0	ε	β	m	ξ	T	ρ
Value	100	150	0.02	100	0.04	0.01	-0.01	0.04	0.005	1	-0.3

For notational convenience, we denote by $\tilde{P}^{\beta,\varepsilon}$ the approximate barrier-option price obtained from the composite expansion in (46), and by P_{MC} the corresponding Monte Carlo benchmark. In all comparisons, the Monte Carlo simulation is performed under the same parameter specification as the approximation. Hence, any observed discrepancy may be interpreted as approximation error rather than model inconsistency.

The Monte Carlo result is computed using the Euler–Maruyama discretisation scheme with 200,000 simulated paths. The time step is set to one trading day, namely

$$\Delta t = \frac{1}{252}.$$

To improve statistical efficiency, antithetic variates are used as a variance reduction technique. In addition, trace plots of the Monte Carlo estimates are inspected to assess convergence. Since barrier crossings may occur between monitoring dates, barrier-option simulations can be affected by discretisation bias. The Monte Carlo values should therefore be understood as high-accuracy numerical proxies for the true model prices. The purpose of the asymptotic formula is not to replace exact valuation methods when they are available, but to provide a fast and accurate approximation that remains reliable over a broad range of parameters.

4.1. Validation Against Monte Carlo Simulation and the Binominal Tree Method

We first validate the approximation against Monte Carlo simulation. The aim is to determine whether the asymptotic formula accurately reproduces both the level and the shape of the barrier-option price when the initial state variables are varied. To this end, we vary the initial asset price S_0 and the initial volatility factor Y_0 separately, while keeping all other parameters fixed at their baseline values.

Figure 1 compares the approximate price $\tilde{P}^{\beta,\varepsilon}$ with the Monte Carlo estimate P_{MC}. Panel (a) reports the dependence of the option value on the initial asset price S_0, while panel (b) shows the effect of varying the initial variance factor Y_0.

In Figure 1a, the initial asset price is varied over the range $96 \leq S_0 \leq 105$. As expected, the up-and-out barrier call price increases with S_0 over this interval. A higher initial asset price increases the likelihood that the option finishes in the money and therefore raises the expected terminal payoff. For an up-and-out contract, however, a higher spot price also brings the asset closer to the barrier level B, increasing the probability of premature knock-

out. The numerical results indicate that, over the range considered, the positive payoff effect dominates the negative barrier effect, so that the option value increases monotonically with S_0.

Figure 1b displays the dependence of the option value on the initial variance factor over the range $0.01 \leq Y_0 \leq 0.02$. The computed prices show that the barrier call value increases with Y_0 over this interval. This behavior is economically intuitive: a higher initial variance increases the dispersion of future asset prices and therefore enhances the upside potential of the payoff $(S_T - K)^+$. Although higher volatility also increases the probability of hitting the upper barrier before maturity, the numerical results suggest that, for the chosen parameter set, the gain from greater upside participation outweighs the loss due to the increased knock-out probability.

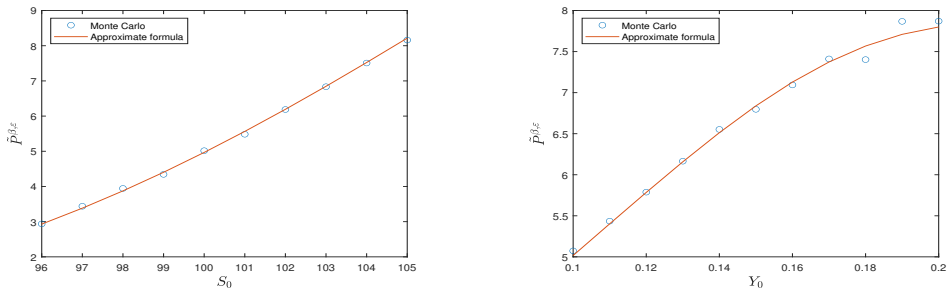

(**a**) (**b**)

Figure 1. Comparison between the approximation $\tilde{P}^{\beta,\varepsilon}$ and the Monte Carlo estimate P_{MC} for the up-and-out barrier call option: (**a**) variation with respect to S_0; (**b**) variation with respect to Y_0.

In both panels, the approximation $\tilde{P}^{\beta,\varepsilon}$ remains very close to the Monte Carlo benchmark. In several regions, the two curves are visually indistinguishable. This indicates that the approximation derived in Corollary 2 is accurate not only at the baseline parameter set, but also under moderate perturbations of the initial state variables. This is important in practical applications, where pricing and calibration routines typically require repeated evaluations over a range of initial conditions.

Moreover, the approximation captures not only the price level but also the local slope of the price curve with respect to both S_0 and Y_0. This suggests that the asymptotic expansion preserves the relevant first-order sensitivity structure of the option value. Such behavior is particularly desirable in hedging, calibration, and comparative statics, where an inaccurate representation of sensitivities may be as problematic as an inaccurate price level.

We also compute barrier-option prices using the binomial tree method considered in [17]. Table 2 compares the computational cost of the closed-form approximation, the binomial tree method, and Monte Carlo simulation. The relative errors are computed with respect to a Monte Carlo benchmark based on 500,000 simulated paths.

Table 2. Comparison of running times and relative errors.

Method	Computation Time	Relative Error
Approximation formula	0.32 s	0.23%
Binomial tree method	4.75 s	0.54%
Monte Carlo simulation, 200,000 paths	31.48 s	0.25%

Table 2 shows that the closed-form approximation is the fastest method and remains very close to the 500,000-path Monte Carlo benchmark. The binomial tree method is also relatively efficient, although its relative error is larger in this experiment. The 200,000-path Monte Carlo simulation provides accurate results, but at a substantially higher compu-

tational cost. These findings highlight the computational advantage of the proposed asymptotic formula, especially in applications requiring repeated price evaluations.

4.2. Sensitivity Analysis

We next analyze the sensitivity of the up-and-out barrier call price to the perturbation parameters ε and β. Recall that ε controls the time scale of the stochastic-volatility factor, while β measures the strength of the elasticity correction in the asset dynamics. The asymptotic analysis is developed under the regime $0 < \varepsilon \ll 1$, $-1 \ll \beta < 0$, and the numerical experiments are therefore conducted in parameter ranges consistent with these assumptions. Specifically, we vary ε between 10^{-3} and 10^{-2}, and β between -10^{-2} and 0.

We first consider the effect of ε. Figure 2a displays both $\tilde{P}^{\beta,\varepsilon}$ and P_{MC} as functions of ε. The option price increases steadily as ε becomes larger over the range considered. Since smaller values of ε correspond to faster mean reversion of the volatility factor, this result indicates that stronger averaging in the volatility dynamics reduces the effective impact of stochastic-volatility fluctuations and lowers the barrier call value. Conversely, when ε is larger, deviations of the variance factor from its long-run level persist for longer, increasing uncertainty in the asset path and raising the option value. The approximation reproduces this monotone trend with high accuracy.

This behavior is consistent with the interpretation of singular perturbation models. In the limit of very small ε, the variance factor mean-reverts so rapidly that the asset effectively experiences an averaged volatility environment. As ε increases, the averaging effect weakens and pathwise stochastic-volatility fluctuations become more pronounced. For a path-dependent derivative such as an up-and-out barrier call, this effect is especially important because volatility influences both the terminal payoff distribution and the probability of hitting the barrier before expiry.

We next examine the elasticity parameter β. Figure 2b shows that the option value increases as β approaches zero from below. Equivalently, a stronger negative elasticity correction reduces the barrier call price. This indicates that the local-elasticity feature encoded by $\beta < 0$ has a price-depressing effect in the present model. The effect is visible even when β is small in magnitude, confirming that the elasticity correction should be retained when accurate barrier-option prices are required. Again, the asymptotic approximation remains in close agreement with the Monte Carlo benchmark over the full parameter range.

From a modeling perspective, the dependence on β is informative because it measures the deviation of the full dynamics from the stochastic-volatility benchmark obtained when the elasticity correction is removed. Since barrier options are highly sensitive to the fine structure of the asset path, even mild local changes in diffusion intensity can materially affect the probability of hitting the upper barrier.

We also investigate the effect of the long-run mean level m. Figure 2c plots both $\tilde{P}^{\beta,\varepsilon}$ and P_{MC} as functions of m. The option price increases as m increases. Since m represents the long-run level of the volatility factor, larger values of m correspond to a higher average variance environment. The resulting increase in volatility enhances the upside potential of the payoff and, for the parameter range considered, raises the up-and-out barrier call value. The approximation again reproduces the monotone trend accurately.

Taken together, the sensitivity experiments show that the approximation captures the effect of the main structural parameters on the option value. This is important because asymptotic formulas may sometimes be accurate at isolated parameter values while failing to preserve correct comparative statics. The present results indicate that the proposed approximation is robust both in price level and in its response to the key model parameters.

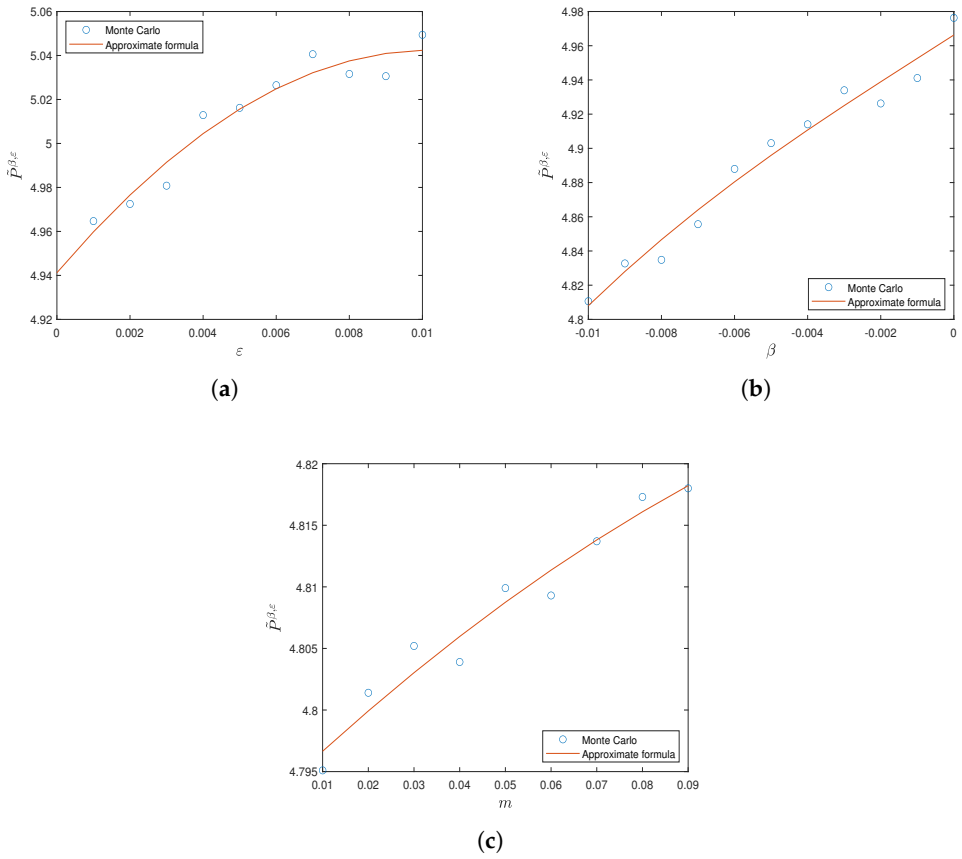

Figure 2. Sensitivity of the up-and-out barrier call option value with respect to the following: (**a**) ε; (**b**) β; (**c**) m.

4.3. Limiting Regimes

We now investigate limiting regimes of the model. These tests serve two purposes. First, they provide further numerical validation of the asymptotic approximation. Secondly, they verify that the approximation is correctly anchored to simpler benchmark models that arise when one or more perturbative effects vanish.

4.3.1. The Regime $\varepsilon \to 0$

We first consider the limit $\varepsilon \to 0$. Under the specification $f(y) = \sqrt{y}$, the fast mean-reverting variance factor is expected to collapse to its long-run average level. Consequently, the full model reduces to an effective constant-volatility benchmark. Formally, the asset-price dynamics in (2) converge to

$$dS_t = rS_t\,dt + f(m)S_t^{1+\beta}\,dW_t^s. \tag{47}$$

Since $f(m) = \sqrt{m}$ is constant, (47) corresponds to the CEV model. Therefore, in the limit of infinitely fast mean reversion, the up-and-out barrier-option price should converge to the corresponding CEV barrier-option price.

This limiting behavior is confirmed numerically in Figure 3a. As ε decreases, the approximation (46) converges towards the benchmark barrier price associated with (47). In the computations, the limiting-model reference value is evaluated using the barrier-pricing approach of [7]. The observed convergence is consistent with the averaging principle underlying the asymptotic expansion and provides an important consistency check for the proposed method.

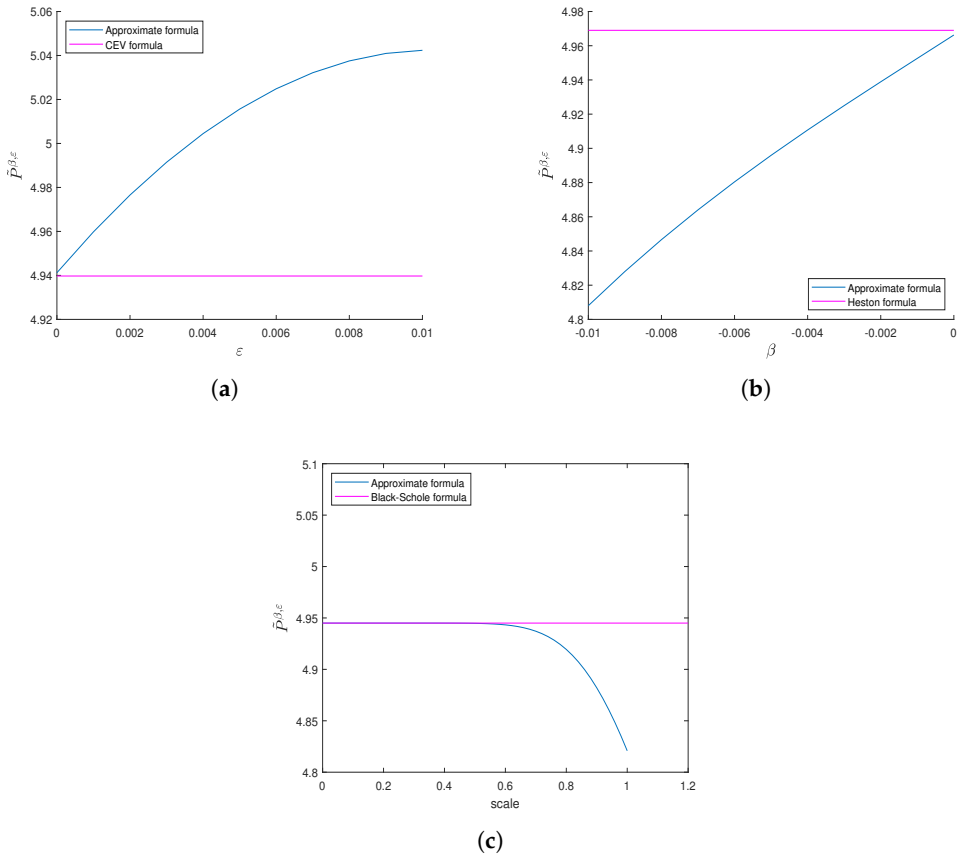

Figure 3. (**a**) Convergence of the approximation (46) to the CEV barrier-option price as $\varepsilon \to 0$. (**b**) Convergence of the approximation (46) to the Heston-type barrier-option price as $\beta \to 0$. (**c**) Convergence of the approximation (46) to the Black–Scholes barrier-option price as $(\varepsilon, \beta) \to (0, 0)$.

This limiting result is not merely a formal reduction. It reflects the central intuition of the asymptotic framework: when volatility fluctuates on a much faster time scale than the option maturity, only its averaged effect remains visible at the pricing level. The numerical convergence to the CEV benchmark therefore provides additional support for the validity of the expansion.

4.3.2. The Regime $\beta \to 0$

We next examine the limit $\beta \to 0$. In this case, the elasticity correction disappears and the asset dynamics reduce to a stochastic-volatility specification of the Heston type:

$$\begin{aligned} dS_t &= rS_t\,dt + f(Y_t)S_t\,dW_t^s, \\ dY_t &= \frac{1}{\varepsilon}(m - Y_t)\,dt + \frac{\sqrt{2\nu}}{\sqrt{\varepsilon}}\,dW_t^y. \end{aligned} \tag{48}$$

With $f(y) = \sqrt{y}$, the asset diffusion coefficient is proportional to $\sqrt{Y_t}S_t$, which is characteristic of stochastic-volatility models of the Heston type. The parameter β therefore measures the deviation of the full model from this stochastic-volatility benchmark.

The numerical results in Figure 3b confirm the expected convergence. As β approaches zero, the approximate price tends to the barrier-option value under the Heston-type model (48). In the computations, this benchmark value is evaluated using the method proposed in [14]. The close agreement between the asymptotic approximation and the benchmark values shows that the expansion captures the correct dependence on the elasticity perturba-

tion and reduces smoothly to the stochastic-volatility model obtained when this correction is removed.

This limiting experiment is particularly useful because it isolates the effect of the elasticity component from that of the fast mean-reverting volatility factor. The results indicate that the approximation separates these two effects correctly, which is a key structural requirement for a valid composite asymptotic formula.

4.3.3. The Joint Regime $(\varepsilon, \beta) \to (0, 0)$

Finally, we consider the joint limiting regime in which both perturbation parameters vanish simultaneously. In this case, both the stochastic-volatility correction and the elasticity correction are removed, and the model reduces to the classical Black–Scholes framework:

$$dS_t = rS_t\,dt + \sqrt{m}\,S_t\,dW_t^s. \tag{49}$$

Thus, the limiting up-and-out barrier call price is the Black–Scholes barrier price with volatility $\sqrt{m}$.

To illustrate this convergence numerically, we impose the scaling

$$(\varepsilon, \beta) = k(0.01, -0.01), \qquad k > 0,$$

and let $k \to 0$. This one-parameter path shrinks both perturbative effects at the same rate and traces the approximation towards the Black–Scholes regime. Figure 3c shows that the approximation converges stably to the Black–Scholes benchmark as k decreases.

This joint-limit experiment confirms that the asymptotic framework is correctly normalized relative to the classical benchmark model. In particular, the approximation performs well not only within the perturbed regime, but also when all additional modeling features vanish. This property is essential for both theoretical consistency and practical reliability.

4.4. Discussion of Numerical Findings

The numerical results lead to several conclusions. First, the approximation $\tilde{P}^{\beta,\varepsilon}$ agrees closely with the Monte Carlo benchmark across all experiments considered. This confirms that the asymptotic expansion is sufficiently accurate for practical pricing purposes within the parameter regime for which it was derived.

Secondly, the approximation reproduces the correct qualitative and quantitative dependence of the option price on the main state variables and perturbation parameters. In particular, it captures the increase in option value with respect to S_0, Y_0, ε, and m, as well as the increase in value as β approaches zero from below. The recovery of these comparative statics indicates that the approximation preserves the main economic mechanisms embedded in the full model.

Thirdly, the limiting-regime experiments show that the approximation converges to the appropriate reduced-model prices as the perturbation parameters vanish. Specifically, the formula is consistent with the CEV benchmark when $\varepsilon \to 0$, with the Heston-type benchmark when $\beta \to 0$, and with the Black–Scholes benchmark when $(\varepsilon, \beta) \to (0, 0)$. These consistency checks provide further support for the theoretical construction of the approximation.

Overall, the numerical evidence demonstrates that the proposed asymptotic formula is accurate, robust, and computationally efficient. It provides a reliable approximation for up-and-out barrier call prices in the stochastic-local volatility setting considered in this paper, while preserving the correct behavior under parameter variation and in the relevant limiting regimes.

4.5. Implementation Remarks

For completeness, we briefly comment on implementation. The asymptotic approximation requires only the evaluation of the leading-order term and the correction terms appearing in the composite expansion (46). Once these components are available in semi-closed form, the computational cost is negligible compared with Monte Carlo simulation. This advantage is especially important when prices must be computed repeatedly, for example across parameter grids or during calibration.

By contrast, Monte Carlo valuation of barrier options is substantially more expensive because entire asset paths must be simulated and barrier crossings must be monitored over time. The cost increases further when a fine time grid is used to reduce missed-crossing bias. The close agreement observed in the numerical experiments therefore suggests that the proposed asymptotic approximation is an attractive alternative in applications where computational speed is essential, provided that the model parameters remain within the perturbative regime assumed in the derivation.

5. Conclusions

In this paper, we have derived a semi-closed form approximate pricing formulae for up-and-out call options in the SVCEV model, through an asymptomatic approach and Fourier transform method. The approximation formulae consists of a leading-order term and the two first-order correction terms. It turns out that the leading-order term is the classical Black–Scholes UOC option price in [22,23], where the constant volatility replaced by the average of stochastic volatility with respect to the invariant distribution of the (hidden) OU-process. We have performed numerical experiments, and our numerical results illustrate that the results from our semi-closed form pricing formula are very close to those generated by Monte Carlo simulation. We have computed up-and-out barrier-option prices using the binomial tree method considered in [17] and compared the computational cost of the closed-form approximation, the binomial tree method, and Monte Carlo simulation. We have also verified the robustness of our model with respect to three perturbation parameters and investigated limiting regimes of the model when one or both perturbative effects vanish. The limiting-regime experiments have showed that the approximation converges to the appropriate reduced prices in some simpler benchmark models, e.g., the CEV, the Heston, or the Black–Scholes model.

Author Contributions: Conceptualization, J.C., X.L. and W.Z.; Methodology, J.C., X.L. and W.Z.; Software, S.G.; Validation, S.G. and W.Z.; Formal analysis, S.G. and W.Z.; Writing—original draft, J.C., X.L., and W.Z.; Writing—review and editing, J.C., S.G., X.L. and W.Z.; Visualization, X.L. and W.Z.; Supervision, J.C. and W.Z.; Project administration, J.C. All authors have read and agreed to the published version of the manuscript.

Funding: This research received no external funding

Data Availability Statement: The original contributions presented in this study are included in the article. Further inquiries can be directed to the corresponding author.

Conflicts of Interest: The authors declare no conflicts of interest.

Appendix A. Derivation of the Identity Using Convolution Theorem

$$\frac{1}{2\pi}\int_{-\infty}^{\infty}\frac{1}{iw}\exp\Big(-\tfrac{1}{2}nw^2+imw\Big)dw=\Phi\Big(\frac{m}{\sqrt{n}}\Big)-\tfrac{1}{2}.$$

$$\frac{1}{2\pi}\int_{-\infty}^{\infty}\frac{1}{1-iw}\exp\Big(-\tfrac{1}{2}nw^2+imw\Big)dw=e^{m+\frac{1}{2}n}\,\Phi\Big(-\frac{m+n}{\sqrt{n}}\Big).$$

We can verify the identities above via convolution. For the first identity, define the integral

$$I(m) = \frac{1}{2\pi}\int_{-\infty}^{\infty} \frac{1}{iw}\,\exp\Big(-\tfrac{1}{2}nw^2 + imw\Big)dw.$$

Interpret this as the inverse Fourier transform of a product. Using the standard definition,

$$I(m) = \mathcal{F}^{-1}\{F(w)G(w)\} = \frac{1}{2\pi}\int_{-\infty}^{\infty} F(w)G(w)e^{iwm}\,dw.$$

Let

$$F(w) = \frac{1}{iw}, \qquad G(w) = \exp\Big(-\tfrac{1}{2}nw^2\Big).$$

The convolution theorem gives

$$I(m) = (f * g)(m) = \int_{-\infty}^{\infty} f(m-y)\,g(y)\,dy.$$

Appendix A.1. Step 1: Identify the Inverse Transform

The inverse transform of $F(w)$ is the sign function:

$$f(y) = \mathcal{F}^{-1}\left\{\frac{1}{iw}\right\} = \frac{1}{2}\,\mathrm{sgn}(y).$$

The inverse transform of the Gaussian is the PDF of $\mathcal{N}(0, n)$:

$$g(y) = \mathcal{F}^{-1}\left\{e^{-\frac{1}{2}nw^2}\right\} = \frac{1}{\sqrt{2\pi n}}\exp\left(-\frac{y^2}{2n}\right).$$

Appendix A.2. Step 2: Evaluate the Convolution

$$\begin{aligned} I(m) &= \frac{1}{2}\int_{-\infty}^{\infty} \mathrm{sgn}(m-y)\,\frac{1}{\sqrt{2\pi n}}\exp\left(-\frac{y^2}{2n}\right)dy \\ &= \int_{-\infty}^{m} \frac{1}{2\sqrt{2\pi n}}e^{-y^2/(2n)}dy - \int_{m}^{\infty} \frac{1}{2\sqrt{2\pi n}}e^{-y^2/(2n)}dy = \Phi\left(\frac{m}{\sqrt{n}}\right) - \frac{1}{2}. \end{aligned}$$

As $n \to 0$, the integral reduces to the inverse Fourier transform of $1/(iw)$, namely $\frac{1}{2}\mathrm{sgn}(m)$, consistent with the result.

For the second identity, let

$$I(m) = \frac{1}{2\pi}\int_{-\infty}^{\infty} \frac{1}{1-iw}\,\exp\Big(-\tfrac{1}{2}nw^2 + imw\Big)\,dw.$$

Take

$$F(w) = \frac{1}{1-iw}, \qquad G(w) = e^{-\frac{1}{2}nw^2}.$$

The inverse Fourier transform of F is

$$f(y) = \mathcal{F}^{-1}\left\{\frac{1}{1-iw}\right\} = e^{y}u(-y),$$

where $u(-y)$ is the Heaviside function equal to 1 for $y \le 0$. As before, the inverse transform of G is

$$g(y) = \frac{1}{\sqrt{2\pi n}}\exp\left(-\frac{y^2}{2n}\right).$$

Appendix A.3. Step 3: Final Expression

$$I(m) = \int_{-\infty}^{0} e^{y} \frac{1}{\sqrt{2\pi n}} \exp\left(-\frac{(m-y)^2}{2n}\right) dy.$$

Combine the exponents:

$$y - \frac{(m-y)^2}{2n} = -\frac{(y-(m+n))^2}{2n} + m + \frac{n}{2}.$$

Then,

$$I(m) = e^{m+\frac{n}{2}} \int_{-\infty}^{0} \frac{1}{\sqrt{2\pi n}} \exp\left(-\frac{(y-(m+n))^2}{2n}\right) dy.$$

With the substitution

$$t = \frac{y-(m+n)}{\sqrt{n}},$$

the integral becomes the standard normal CDF, giving the final result:

$$I(m) = e^{m+\frac{n}{2}} \Phi\left(-\frac{m+n}{\sqrt{n}}\right).$$

As $n \to 0$, this reduces to the inverse transform of $\frac{1}{1-iw}$, which is $e^{m}u(-m)$, consistent with the limiting behavior.

References

1. Merton, R. The theory of rational option pricing. *Bell J. Econ. Manag. Sci.* **1973**, *1*, 141–183.
2. Black, F.; Scholes, M. The pricing of options and corporate liabilities. *J. Political Econ.* **1973**, *3*, 637–654.
3. Reiner, E.; Rubinstein, M. Breaking down the barriers. *Risk* **1991**, *4*, 28–35.
4. Cox, J. *Notes on Option Pricing I: Constant Elasticity of Variance Diffusions*; Working Paper; Stanford University: Stanford, CA, USA, 1975.
5. Heston, S.L. A closed-form solution for options with stochastic volatility with applications to bond and currency options. *Rev. Financ. Stud.* **1993**, *2*, 327–343.
6. Boyle, P.P.; Tian, Y. Pricing lookback and barrier options under the CEV process. *J. Financ. Quant. Anal.* **1999**, *34*, 241–264.
7. Davydov, D.; Linetsky, V. Pricing and hedging path-dependent options under the CEV process. *Manag. Sci.* **2001**, *47*, 949–965.
8. Thakoor, N.; Tangman, D.Y.; Bhuruth, M. Efficient and high accuracy pricing of barrier options under the CEV diffusion. *J. Comput. Appl. Math.* **2014**, *259*, 182–193.
9. Carr, P.; Itkin, A.; Muravey, D. Semi-closed form prices of barrier options in the time-dependent CEV and CIR models. *J. Deriv.* **2020**, *28*, 1–25.
10. Chiarella, C.; Kang, B.; Meyer, G.H. The evaluation of barrier option prices under stochastic volatility. *Comput. Math. Appl.* **2012**, *64*, 2034–2048.
11. Kato, T.; Takahashi, A.; Yamada, T. An asymptotic expansion formula for up-and-out barrier option price under stochastic volatility model. *Jpn. Soc. Ind. Appl. Math. Lett.* **2013**, *5*, 17–20.
12. Hagan, P.S.; Kumar, D.; Lesniewski, A.; Woodward, D.E. Managing smile risk. *Wilmott Mag.* **2002**, *1*, 84–108.
13. Carr, P.; Itkin, A.; Muravey, D. Semi-analytical pricing of barrier options in the time-dependent Heston model. *arXiv* **2022**, arXiv:2202.06177.
14. He, X.; Lin, S. An analytical approximation formula for barrier option prices under the Heston model. *Comput. Econ.* **2022**, *60*, 1413–1425.
15. Cao, J.; Kim, J.-H.; Li, X.; Zhang, W. Valuation of barrier and lookback options under hybrid CEV and stochastic volatility. *Math. Comput. Simul.* **2023**, *208*, 660–676.
16. Choi, S.-Y.; Fouque, J.-P.; Kim, J.-H. Option pricing under hybrid stochastic and local volatility. *Quant. Financ.* **2013**, *13*, 1157–1165.
17. Peng, B.; Peng, F. Pricing arithmetic Asian options under the CEV process. *J. Econ. Financ. Adm. Sci.* **2010**, *15*, 7–13.
18. Kim, J.-H.; Yoon, J.-H.; Lee, J.-H.J.; Choi, S.-Y. On the stochastic elasticity of variance diffusions. *Econ. Model.* **2015**, *51*, 263–268.
19. Cao, J.; Kim, J.-H.; Zhang, W. Pricing variance swaps under hybrid CEV and stochastic volatility. *J. Comput. Appl. Math.* **2021**, *386*, 113220.
20. Fouque, J.-P.; Papanicolaou, G.; Sircar, R. *Derivatives in Financial Markets with Stochastic Volatility*; Cambridge University Press: Cambridge, UK, 2000.

21. Fouque, J.-P.; Papanicolaou, G.; Sircar, R.; Sølna, K. *Multiscale Stochastic Volatility for Equity, Interest Rate, and Credit Derivatives*; Cambridge University Press: Cambridge, UK, 2011.
22. Hull, J. *Options, Futures and Other Derivatives*, 9th ed.; Options; Pearson: Sydney, Australia, 2015.
23. Haug, E. *The Complete Guide to Option Pricing Formulas*, 2nd ed.; McGraw-Hill: Sydney, Australia, 2006.